한국부식학회지
J. Corros. Sci. Soc. of Korea
Vol. 18, No. 2, June, 1989
〈研究論文〉

Enhanced Diffusion of Oxygen During Internal Oxidation of Iron Based Alloys

Jeong Y·Lee

Department of Materials Science and Engineering, Korea Institute of Technology

Iron-base alloys, Fe-1%Al, Fe-1%Al-1%Hf, Fe-1%Cr, Fe-1%Cr-1%Hf and Fe-2%Hf, were oxidized in a sealed quartz tube in the oxygen atmosphere produced by the decomposition of FeO in the mixture of Fe/FeO powder at 800°C for the various time periods of 2 hours to 121 hours.

Results show that the variation of the solute element and the addition of Hf in the iron-base alloys led to a significant change in the depth of internal oxidation zone and in the internal oxide distributions. The ratios of the apparent diffusion coefficient of oxygen in the internal oxidation zone and the diffusion coefficient of oxygen in the alloy lattice were 14.4-42.0. In attempting to interpret the dependence of the oxide growth rate on the internal precipitate distributions, a model incorporating enhanced diffusion of oxygen along the incoherent interface between the internal oxide particles and the alloy matrix was proposed.

It is concluded, from the agreement between experimental results and the model, that the incoherent interface between the oxide and the alloy matrix is effective for inward oxygen diffusion in the internal oxidation zone at this temperature.

1. INTRODUCTION

Iron-based alloys, which have been proposed for use in coal gasification processes may corrode quickly if they are unable to form a protective, slowly growing, external scale. At the same time, oxygen can diffuse into the alloy and precipitate as an oxide which would normally form a protective scale. The process of an oxide being precipitated within the alloy due to the inward diffusion of oxygen is termed internal oxidation.

The models of internal oxidation have changed progressively over the past years. Wagner[1] developed general equations for internal oxidation of a dilute binary alloy, taking into account the diffusion of oxygen inwards and of the alloying element outwards. Rapp[2] and others[3),4] expanded this treatment, still using a pseudo-binary approach, but pointing out two limiting cases. These classical models of internal oxidation have generally been successful in describing the internal oxidation behavior of a

wide range of dilute alloys, in which the solute metal forms a more stable oxide than the solvent metal.

The internal oxidation of alloys occurs through the dissolution of atomic oxygen into the base metal at the external surface (in the absence of an external oxide scale) or at the metal/external scale interface. The dissolved oxygen diffuses inward through the base metal matrix containing a given volume fraction of previously precipitated internal oxide particles. At an advancing reaction front which remains essentially parallel to the original surface, the inward diffusion of oxygen and the outward diffusion of the alloying element continuously provide oxygen and alloying element concentrations in excess of those corresponding to the solubility product of the alloying element oxide in the base metal matrix. Since the solute oxide is very stable, the concentrations of solute remaining dissolved in the alloy within the internal oxidation zone, and of oxygen beyond the internal oxidation zone, should be very low. A repeated nucleation with some accompanying growth of particles of the alloying element oxide results, and the reaction front continues to advance inward at a decreasing rate, which may be calculated if the simple model is assumed to hold. By solving the transport equation under these conditions, assuming that the previously precipitated internal oxides do not interfere with the inward diffusion of oxygen, the rate of advancement of the internal oxide front can be related to the fundamental variables:[5] oxygen diffusivity in the metallic matrix of the internal oxidation zone, which is essentially pure solvent as outlined above, the metallic interdiffusion coefficient of the alloy, the oxygen solubility of the solvent, the solute content of the alloy, and the stoichiometric ratio of oxygen to solute in the oxide precipitate. In fact, measurements of internal oxidation rates are frequently used to determine oxygen permeabilities (product of solubility times diffusivity) in metals.[6),7)]

Previous researches[8),9),10),11),12)] have shown that the small addition of active element Hf in the alloy, significantly improved the adhesion of the scale to the metal. The formation of inwardly gorwing oxide pegs is known as a main factor for the scale adhesion under both isothermal and particularly thermal cycling condition.[10),11)] The improved scale adherence is mainly attributed to the mechanical keying of the scale to the substrate caused by the development of oxide intrusions which penetrate into the alloy. These intrusions are formed of the internal oxides which grow inwardly, encapsulating the reactive element oxide particles and are thus connected to the external scale.[8)]

In attempting to interpret peg formation, it was suggested[10),11)] that Al_2O_3 scale grows inwardly in the alloy encapsulating the HfO_2 particle via enhanced oxygen diffusion along the supposedly incoherent interface between the oxide particles and the alloy matrix. However, in addition, the incoherent α/β phase boundaries also appear capable of acting as easy paths for the inward growth of the oxide.[12)] Recently, it was proposed a model[5)] incorporating enhanced diffusion of oxygen along the incoherent interface between the internal oxide particles and the alloy matrix in nickel-base alloys. Agreement between experiment and theory was satisfactory if the ratio of diffusion of coefficients in the interface

and the bulk lattice is of the order of 10^2-10^3 in the Ni-Al system and approximately 10^4 in the Ni-Cr system. [5)]

The objective of the present research is to study the feasibility of the enhanced oxygen diffusion along the interface between the internal oxide precipitates and the alloy matrix, and its possible influence on the growth mechanism by directly examing the relationship between the growth rate and morphology of the internal oxides at 800°C in iron-base alloys.

2. EXPERIMENTAL PROCEDURE

The Fe-base alloys used in this research were Fe-1%Al, Fe-1%Al-1%Hf, Fe-1%Cr, Fe-1%Cr-1% Hf and Fe-2%Hf (all in wt.%). The reasons for the choice of the alloys were as follows: (1) The variation of the solute element and the addition of Hf were more effective in modifying the internal oxide morphology than the variation of the solute content. Increasing the solute content led to an increase in the internal oxide size and volume fraction. (2) The free energy of formation for Al_2O_3, Cr_2O_3, HfO_2 is much more negative than that of FeO, the lowest oxide of iron metal. In order to achieve the required activity of dissolved oxygen at the reaction front, the pure solvent metal, iron exhibits a significant solubility and diffusivity for atomic oxygen in its lattice at the temperature of oxidation. So the element Al, Cr, Hf can form internal oxide in the alloy and the solubility product of oxide in the alloy is negligible. (3) The solute content must be small so that the diffusivity is independent of the concentration. And the solute metal content must be lower than the concentration to cause the transition from internal to external oxidation. But it must be enough to observe the enhanced diffusion effect if it exists.

The alloys were prepared by vacuum melting in a high frequency induction furnace and casting into cylindrical molds of 3x28 cm. All the alloys listed above were cut in small rectangular sample of 15x10x3mm. Internal oxidation was carried out in a Rhines pack, using Fe/FeO powder mixtures as the source of oxygen. The oxygen pressure inside the reaction tube was set by the Fe/FeO mixture maintained at the reaction temperature. Care was taken to grind the mixture and mix with a small amount of Fe, in order to avoid oxidizing the FeO to Fe_3O_4, after each experiment in preparation for the following one.

For internal oxidation without external scale, the oxygen partial pressure in the environment must be greater than that required to oxidize the alloying element but less than required to form FeO. The relative contribution of the interface boundary diffusion diminishes rapidly with temperature, so the oxidation temperature must be low in the temperature range, where the high temperature corrosion is the major problem. Thus, the specimens were oxidized in the sealed quartz tube containing Fe/FeO powder mixtures at 800°C for the various time periods of 2 hours to 121 hours.

Depths of internal oxidation were measured in an optical microscope from metallographically prepared cross-sections. The oxide particle size and area fraction were evaluated from sections parallel to the original alloy surface, around the middle of the internal oxidation zone. The specimens were etched by partial selective alloy dissolution in a 10% bromine-methyl alcohol solution at 40°C for five minutes, technique devised to examine the morphology of internal

oxide precipitates. These specimens were subsequently gold plated for observation under a scanning electron microscope.

The determination of the composition of the oxide precipitate within the internal oxidation zone was based on energy dispersive x-ray microanalysis and x-ray diffraction analysis. To minimize interference from the substrate, the measurements were performed on deeply-etched specimens.

3. RESULTS AND DISCUSSION

Figure 1 shows the depths of the internal oxidation front, measured from the alloys/gas interface, as a function of the square root of time for the five iron-base alloys. Since the samples were oxidized in a sealed quartz tube in the oxygen atmosphere produced by the decomposition of FeO in the mixture of Fe/FeO powder at 800°C, any external scale was not observed in the optical and scanning electron micrographs. The plot has been made with the assumption of the parabolic rate law by plotting x, the depth of the zone of internal oxidation, versus the square root of time, $\sqrt{t}$. A straight line is then forced through the points defined for each sample and the values of the slope were calculated by the least square method. It can be noted that the greatest slope, that is, $x/\sqrt{t}$, is obtained with Fe-2% Hf alloy and the smallest with Fe-1%Al alloy. It is known that the small addition of Hf reduces the overall oxidation rate,[9] which includes the external oxide growth rate. However, it is evident that the addition of Hf to Fe-1%Al slightly increased the slope, that is, the internal oxide growth rate. And the addition of Hf to Fe-1%Cr significantly affected the slope as shown in Fig. 1.

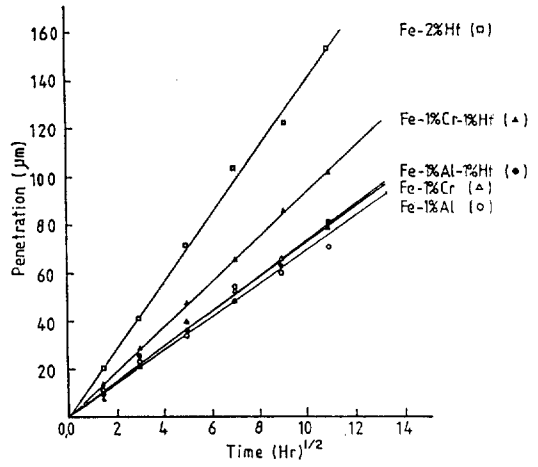

Fig. 1. Parabolic plot of internal oxidation zone growth.

According to the analysis of Wagner,[13] if the kinetics of the reaction are diffusion controlled, the depth of the internal oxidation zone, $\bar{x}$, varies linearly with the square root of time.

$$\bar{x} = 2\gamma (D_O t)^{1/2} \tag{1}$$

where D_O is the diffusivity of oxygen in the base metal and γ is a dimensionless parameter dependent on the relative contribution of the diffusion of the component being internally oxidized in the internal oxidation zone, or in another form,

$$\bar{x} = k\sqrt{t} \tag{2}$$

where k is the parabolic rate constant for the advance of the internal oxidation zone. Using Fick's second law, for the one dimensional case of oxygen diffusion,

$$\frac{\partial N_O}{\partial t} = \frac{\partial^2 N_O}{\partial x^2} \tag{3}$$

where the boundary conditions are:

$$N_O = N_O^{(s)} \text{ for } x = 0, t > 0 \tag{3a}$$

$$N_O = 0 \text{ for } x \geq \bar{x}, t > 0, \tag{3b}$$

where x is the distance from the alloy surface, and N_O and $N_O^{(s)}$ are the mole fractions of dissolved oxygen in the base metal and of oxygen at the external surface respectively. Using Fick's second law once again for the active element B,

$$\frac{\partial N_B}{\partial t} = \frac{\partial^2 N_B}{\partial x^2} \tag{4}$$

with the boundary conditions

$$N_B = N_B^{(o)} \text{ for } x = 0, t = 0 \tag{4a}$$

$$N_B = 0 \text{ for } x \leq \bar{x}, t > 0, \tag{4b}$$

where N_B and $N_B^{(o)}$ are the mole fractions of B in the internal oxidation zone and of B in the original base metal respectively. The solutions to equation (3) and (4) are:

$$N_O = N_O^{(s)} \left\{ 1 - \frac{erf[x/(D_O t)^{1/2}]}{erf(\gamma)} \right\} \tag{5}$$

$$N_B = N_B^{(o)} \left\{ 1 - \frac{erfc\,[x/(D_B t)^{1/2}]}{erfc\,(\gamma\phi^{1/2})} \right\} \tag{6}$$

where $\phi = D_O/D_B$ is the ratio of lattice diffusion coefficients of oxygen to B in the alloy. At the internal oxidation front, the flux of oxygen atoms arriving from the external surface must be equivalent to the flux of B atoms arriving from the bulk alloy, if an insoluble and stoichiometric BO_ν particle is precipitated:

$$\lim_{\varepsilon \to o} \left[-D_O \left(\frac{\partial N_O}{\partial x}\right)_{x=x-\varepsilon} = \nu D_B \left(\frac{\partial N_B}{\partial x}\right)_{x=x+\varepsilon} \right] \tag{7}$$

where ν is the ratio of O/B atoms in the oxide. Subsituting equations (5) and (6) into Equation (7) and rearranging the statement yields:

$$\frac{N_O^{(s)}}{\nu N_B^{(o)}} = \frac{\exp(\gamma^2)\, erf(\gamma)}{\phi^{1/2} \exp(\gamma^2 \phi) erfc\,(\gamma\phi^{1/2})} \tag{8}$$

Thus, if equation (7) and the boundary conditions (3) and (4) are valid and all the quantities of equation (8) are known except γ, γ may be obtained via graphical or numerical analysis. once γ is obtained, the diffusivity of oxygen can be calculated from equations (1) and (2).

Usually, equation (8) is used in one of two limiting forms: (a) for the first limiting case, when $\gamma \ll 1$ and $\gamma\phi^{1/2} \gg 1$, equivalent to $D_B/D_O \ll N_O^{(s)}/N_B^{(o)} \ll 1$ and

$$\gamma \approx \left[\frac{N_O^{(s)}}{2\nu N_B^{(o)}} \right]^{1/2} \tag{9}$$

and (b) for the second limiting case, $\gamma \ll 1$ but $\gamma\phi^{1/2} \ll 1$, equivalent to $N_O^{(s)}/N_B^{(o)} \ll D_B/D_O \ll 1$ and

$$\gamma \approx \frac{(\pi\phi)^{1/2} N_O^{(s)}}{2\nu N_B^{(o)}} \tag{10}$$

These two limiting cases also correspond to (a) insignificant diffusion of component B during the internal oxidation process and consequently no enrichment of B in the internal oxidation zone, and (b) significant diffusion of component B during the internal oxidation process and hence its enrichment within the internal oxidation zone respectively.

Table 1 shows relevant solubility and diffusivity data in iron-base alloys. From these solubility and diffusivity data, it is possible to determine which limiting case is applicable to the present systems.

Table 1. Solubility and diffusivity values in Fe-base alloys.

Diffusivity of O in Fe[15]	3.4×10^{-9}	cm^2/sec
Diffusivity of Al in Fe[16]	1.0×10^{-11}	cm^2/sec
Diffusivity of Cr in Fe[17]	5.4×10^{-12}	cm2/sec
Diffusivity of Hf in Fe[18]	1.0×10^{-14}	cm^2/sec

However, in the Fe-Al system, estimations of the ratios D_{Al}/D_O and $N_O^{(s)}/N_B^{(o)}$ were very similar as $D_{Al}/D_O = 2.9\times10^{-3}$ and $N_O^{(s)}/N_B^{(o)} = 1.2\times10^{-3}$ for the Fe-1%Al alloy. However, as shown later, D_O may well be altered by the inferface between the internal oxide and the matrix alloy, whereas this is unlikely with D_{Al} since aluminum diffusion is only significant in the alloy below the precipitation front. Thus, a clearer distinction between the two limiting cases is possible using the experimentally determined internal oxidation depths. From equation (1) and the ratio $\phi = D_O/D_B$, it is seen that

$$\gamma\phi^{1/2} = \bar{x}/2\sqrt{D_{Al}\,t} \tag{11}$$

Rewriting equation (8) as

$$\frac{N_O^{(s)}}{\nu N_B^{(o)}} = \frac{\exp(\gamma^2)erf(\gamma)}{F(\gamma\phi^{1/2})} \tag{12}$$

where the auxiliary function $F(\gamma\phi^{1/2})$ has been defined by Wagner[1] and noting that under all conditions $\gamma\phi^{1/2} > 2$, and $F(\gamma\phi^{1/2}) > 0.9 \approx 1$, gives

$$\frac{N_O^{(s)}}{\nu N_B^{(o)}} = \exp(\gamma^2)\,erf(\gamma) \tag{13}$$

Using the solubility data in Table 1 and $\nu = 1.5$ for Al_2O_3 gives

$$\frac{N_O^{(s)}}{\nu N_B^{(o)}} = \exp(\gamma^2)erf(\gamma) \approx 7.8\times10^{-4} \tag{14}$$

and hence $\gamma \ll 1$. Thus, in the Fe-Al system, the first limiting case is valid, that is, the growth rate is controlled by the inward diffusion of oxygen with negligible outward diffusion of aluminum.

In the Fe-Cr system, the diffusivity of Cr in the alloy is about one order of magnitude lower than that of aluminum as shown in Table 1, and it can be expected that the first limiting case is valid. In the Fe-Hf system, the diffusivity of Hf in the alloy is about three orders of magnitude lower than that of aluminum (see Table 1), and consequently the first limiting case is also valid. Thus, in all cases in this study, the parabolic rate constant for the advance of the internal oxidation zone, k, is given by combination of equations (1), (2) and (9) as

$$k = \frac{\bar{x}}{\sqrt{t}} = \left[\frac{2N_O^{(s)} D_O}{\nu N_B^{(o)}}\right]^{1/2}. \tag{15}$$

The ratio of oxygen to B component in the stoichiometric precipitate has a value of 1.5 in the Fe-Al and Fe-Cr systems since the precipitate oxide is primarily either Al_2O_3 or Cr_2O_3. However, a value of ν of 2.0 in the Al-Hf system, corresponding to HfO_2 was used to calculate the oxygen permeability product (solubility x diffusivity product). The composition of the oxide precipitates within the internal oxidation zone was determined by energy dispersive x-ray analysis and x-ray diffraction analysis. The parabolic rate constants, which were measured from the slopes in Fig. 1, are included in Table 2. From these data, the oxygen permeability product $N_O^{(s)}D_O$ was calculated from equation (15). Since, as shown later, D_O may well be altered by the interface between the internal oxide and the matrix alloy, the apparent oxygen diffusivity, $D_{O,app}$, was calculated using the value of the oxygen solubility in Table 1. Values are also included in Table 2.

Table 2 shows that the apparent diffusivity values increase with adding Hf in the alloys and the apparent diffusivity value obtained from the Fe-2%Hf is greatest. In order to understand this apparent increase in diffusivity it is appropriate to consider the morphology of the internal oxide precipitates.[18)]

Figure 2 shows typical transverse sections which were taken on deeply-etched samples with a 10% bromine-methyl alcohol solution on a scanning electron microscope. In the Fe-Al system, the internal oxide precipitates tend to be acicular in nature, orientated perpendicularly to the original alloy surface, whereas in the Fe-Cr and Fe-2%Hf systems the precipitates are polyhydral and spherical in shape, respectively. In the Fe-1%Al alloy, the precipitates adopted the form of needles with several branches. Notice that there is a relatively denser population of precipitates at this alloy grain boundary due to preferential heterogeneous nucleation of the internal oxide at the grain boundary, as shown in the Fe-1%Cr alloy in Fig 2. In contrast to the needle-like precipitates formed in the Fe-1%Al and Fe-1%Al-1%Hf alloys, the addition of Hf to the Fe-1%Cr alloy did not lead to a noticeable morphological change as shown in Fig. 2.

Table 2. Experimental and calculated data for the internal oxidation of Fe-base alloys.

Alloy	kx10^5 cm/$\sqrt{sec}$	$D_{O,app}$x10^8 cm^2/sec	$D_{O,app}/D_{O,m}$	rx10^4 cm	A_{ox}	(A_i/d)x10^{-4} cm^{-1}
Fe-1%Al	1.15	8.50	25.0	0.38±0.06	0.426	2.24
Fe-1%Al-1%Hf	1.22	9.56	28.1	0.33±0.12	0.467	2.83
Fe-1%Cr	1.19	4.91	14.4	1.23±0.31	0.224	0.36
Fe-1%Cr-1%Hf	1.56	8.20	24.1	0.97±0.17	0.310	0.64
Fe-2%Hf	2.32	14.3	42.0	0.28±0.05	0.558	3.18

k: precipitate growth rate constant, $D_{O,app}$: apparent oxygen diffusivity, r: average particle radius, A_{ox}: area fraction of oxide, A_i: area fraction of interface, d: width of interface.

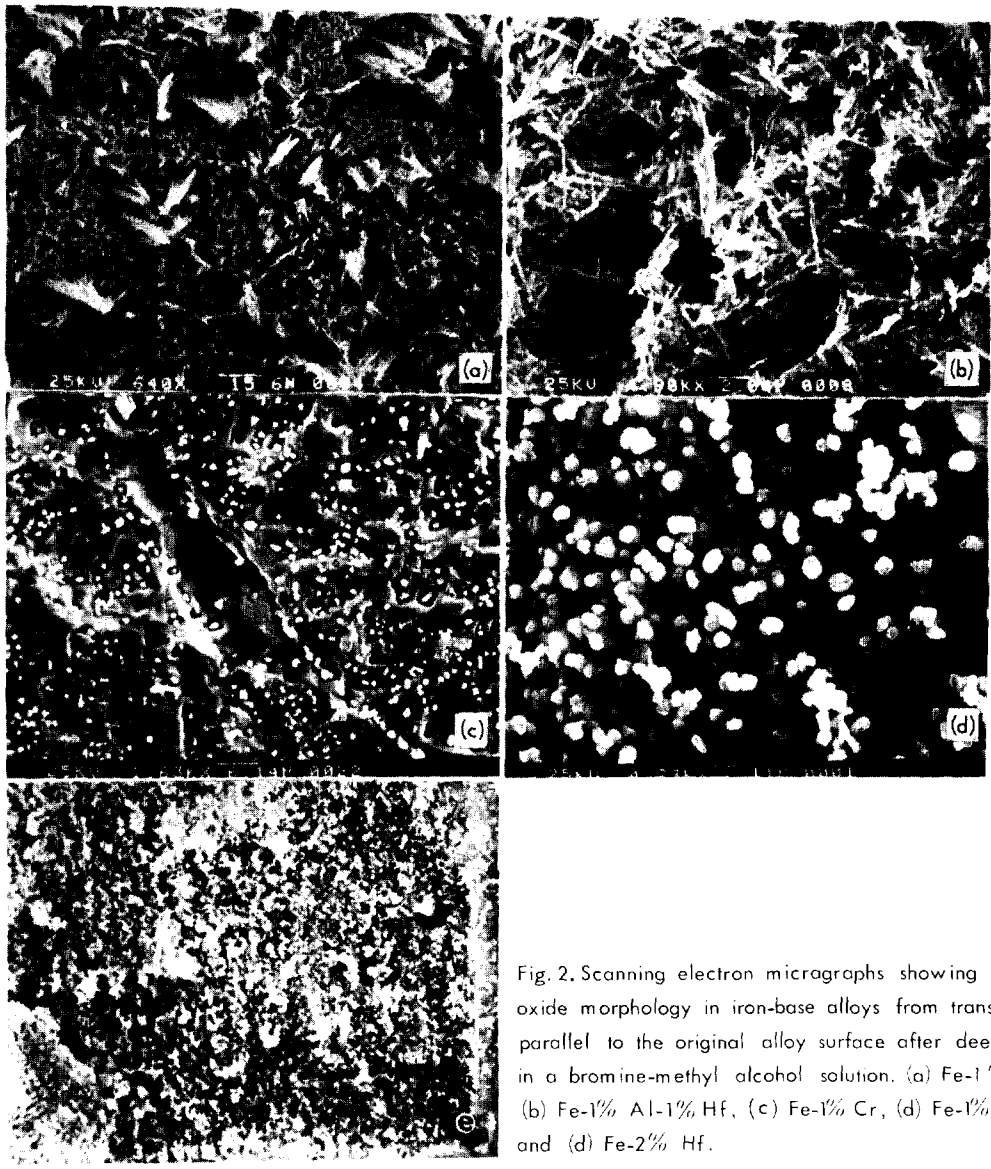

Fig. 2. Scanning electron micrographs showing internal oxide morphology in iron-base alloys from transverse sections parallel to the original alloy surface after deeply etching in a bromine-methyl alcohol solution. (a) Fe-1%Al, (b) Fe-1% Al-1% Hf, (c) Fe-1% Cr, (d) Fe-1% Cr-1% Hf and (d) Fe-2% Hf.

If oxygen diffusion within the internal oxidation zone is enhanced along the incoherent interface between the internal oxide particles and the alloy matrix, the apparent flux of oxygen through the internal oxidation zone is considered as the sum of the fluxes of oxygen through the alloy matrix, J_m, the internal oxide/matrix interface, J_i, and the internal oxide precipitates themselves, J_{ox}. Thus,

$$J_{app} = J_m A_m + J_i A_i + J_{ox} A_{ox} \qquad (16)$$

where A_m, A_i and A_{ox} are area fractions of alloy matrix, interface and internal oxide in a unit

cross-sectional area parallel to the original alloy surface. Since oxygen diffusivities in the internal oxides themselves are very small in compared to those in the alloy matrix and the incoherent interface, the third term in equation (16) can be neglected. Then the apparent diffusion coefficient for oxygen in the internal oxide zone is defined as

$$D_{O,app} = D_{O,m}A_m + D_{O,i}A_i \qquad (17)$$

where $D_{O,m}$ is the diffusion coefficient of oxygen in the alloy matrix and $D_{O,i}$ the diffusion coefficient in the incoherent interface. Since the interface width, d, is presumably taken as several interatomic distances, the area fraction of the interface is negligible in comparison to the area fractions of alloy matrix and oxide. Thus,

$$D_{O,\,app} = D_{O,\,m}(1-A_{ox}) + D_{O,i}A_i \qquad (18)$$

and

$$\frac{D_{O,app}}{D_{O,m}} = (1-A_{ox}) + \frac{D_{O,i}}{D_{O,m}} A_i \qquad (19)$$

Both these diffusion coefficients are assumed independent of composition. The ratio, $D_{O,app}/D_{O,m}$, is expected to increase with the increase of the area fractions of interface and alloy matrix. The ratio, $D_{O,app}/D_{O,m}$, was calculated using the value of the oxygen diffusivity in Table 1. Values are given in Table 2. The ratios, $D_{O,app}/D_{O,m}$, show relatively high values ranging from 14.4 in the Fe-Cr alloy to 42.0 in the Fe-Hf alloy in Table 2, which implies that there is a large enhancement of oxygen diffusion in the internal oxidation zone. Thus, it is appropriate to consider that oxygen diffusion is enhanced along the defects, most probably the in coherent oxide/matrix interface, in the internal oxidation zone.

The area fractions, A_{ox} and A_i, depend, among other factors, on the morphology of the internal oxides. For evaluation of these fractions from the scanning electron micrographs, it is assumed that the internal oxides in the Fe-Cr system take the form of discs in a cross-sectional plane parallel to the external surface. The radius of the discs, spheres and needles is designated r. In fact, instead of the area fraction of the interface, the apparent oxide/matrix interface boundary density, which is designated A_i/d, was calculated using the measured distributions. The measurements included all particles on at least 20 scanning electron micrographs. The results are shown in Table 2. For this evaluation, the specimens were slightly etched in a 1% bromine-methyl alcohol solution at room temperature since deeply-etched specimens revealed the internal oxides themselves rather than the internal oxide/alloy interface. Typical transverse sections which were used for evaluation for all alloy compositions are included in Fig. 3. They clearly show that there is a remarkable difference in the distribution of the internal oxides. There is a relatively large variation in boundary density with a significant difference in internal oxide distribution, which arose from varying alloy composition and active element addition.

By comparing the apparent oxygen diffusivities with the apparent oxide/matrix interfacial boundary densities in Table 2, it clearly shows that there is a significant variation in boundary density with the apparent oxygen diffusivity. For instance, increasing the ratio, $D_{O,app}/D_{O,m}$,

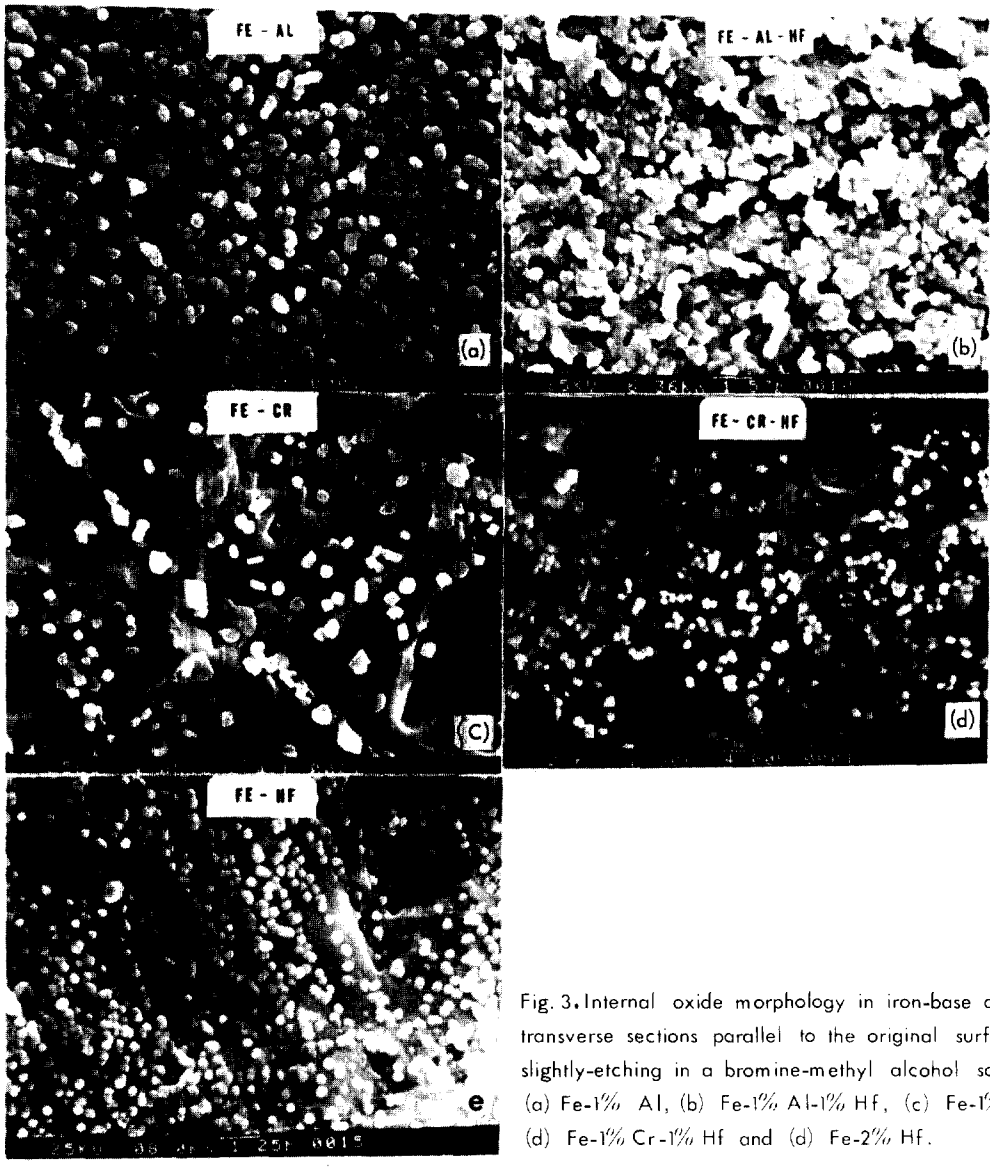

Fig. 3. Internal oxide morphology in iron-base alloys fron transverse sections parallel to the original surface after slightly-etching in a bromine-methyl alcohol solution. (a) Fe-1% Al, (b) Fe-1% Al-1% Hf, (c) Fe-1% Cr, (d) Fe-1% Cr-1% Hf and (d) Fe-2% Hf.

from 14.4 in the Fe-Cr alloy to 42.0 in the Fe-Hf alloy led to an increase in the interfacial boundary density from 0.36×10^4 cm^{-1} in the Fe-Cr alloy to 3.18×10^4 cm^{-1} in the Fe-Hf alloy. Thus, it seems appropriate to consider that the dependence of the apparent oxygen diffusivity on the interfacial density infers that the incoherent interface between the internal oxide and the alloy matrix enhanced oxygen diffusion, that is, the internal oxide growth was controlled by oxygen diffusion, most probably along the interfacial boundary, at this temperature. The deviations from the expected dependence of the apparent oxygen diffusivity on the interfacial density might be due to the fact that the true boundary density would be greatly different.

since the actual interface width depends on the degree of incoherency.

Previous investigations.[10),11)] have shown that Al_2O_3 scale grows inwardly in the alloy via enhanced oxygen diffusion along the supposedly incoherent interface between the oxide particles and the alloy matrix. Furthermore, the incoherent α/β phase boundaries also appear capable of acting as easy paths for the inward growth of the oxide.[12)] In nickel-base alloys, it has been shown[5)] that the internal oxides grow by enhanced diffusion of oxygen along the incoherent interface between the internal oxide particles. Results of the present research are consistent with those of these previous investigations.

4. CONCLUSIONS

The variation of the solute element and the addition of Hf in the iron-base alloys led to a significant change in the depth of internal oxidation zone and in the internal oxide distributions. The ratios of the apparent diffusion coefficient of oxygen in the internal oxidation zone and the diffusion coefficient of oxygen in the alloy lattice were 14.4-42.0. In attempting to interpret the dependence of the oxygen diffusivity on the internal precipitate distributions, a model incorporating enhanced diffusion of oxygen along the incoherent interface between the internal oxide particles and the alloy matrix was proposed. It is concluded, from the agreement between experimental results and the model, that the incoherent interface between the oxide and the alloy matrix is effective for inward oxygen diffusion in the internal oxidation zone at this temperature.

REFERENCES

1. C. Wagner, *Z. Electrochem.*, **63**, 663 (1959).
2. R.A. Rapp, *Corrosion*, **21**, 382 (1965).
3. J.L. Meijering, *Adv. in Materials Research*, **5**, edited by H. Herman, Academic Press, New York, 1971.
4. J.H. Swisher, *Oxidation of Metals and Alloys*, edited by D.L. Douglass, ASM, Metals Park, Ohio, 1971.
5. D.P. Whittle, Y. Shida, G.C. Wood, F.H. Stott, and B.D. Bastow, *Lawrence Berkeley Laboratory Report*, LBL-13521, LBL, Berkeley, CA, Oct., 1981.
6. R. Barlow, P.J. Grundy and B. Johnson, *J. Mater. Sci.*, **4**, 359 (1969).
7. M.T. Hepworth, R.P. Smith and E.T. Turkdogan, *Trans. Met. Soc. AIME*, **238**, 236 (1966).
8. J.K. Tien and F.S. Pettit, *Met. Trans.*, **3**, 1587 (1972).
9. D.P. Whittle and J. Stringer, *Phil. Trans. Roy. Soc., London*, **A295**, 309 (1980).
10. I.M. Allam, D.P. Whittle and J. Stringer, *Oxid. Met.*, **13**, 381 (1974).
11. H. Hindam and D.P. Whittle, *J. Electrochem. Soc.*, **129**, 129 (1982).
12. D.P. Whittle and D.H. Boone, *Proc. of 7th LBL/MMRD International Materials Symposium, Surfaces and Interfaces in Ceramic and Ceramic-Metal System*, Lawrence Berkeley Laboratory, Berkeley, CA, Jul 28-30, 1980.
13. R.A. Rapp, *21st Conf. National Association of Corrosion Engineers*, NACE, St. Louis, Mo., Mar. 15-19, 1965.
14. J.H. Swisher and E.T. Turkdogan, *Trans. AIME*, **239**, 426 (1967).

15. R. Barlow and P.J. Grundy, *J. Mater. Sci.*, **4**, 797 (1969).
16. A. Vignes, *Trans. 2nd Natl. Conf. Electron Microprobe Analysis,* Paper No. 20, Boston, 1967.
17. A.W. Bowen and G.M. Leak, *Met. Trans.* **1**, 1696 (1970).
18. H. Hindam and D.P. Whittle, *Proc. of JIM Third International Symposium on High Temperature Corrosion of Metals,* Tokyo, Japan, Nov. 17-20, 1982.